# Mapping the depth dependence of shear properties in articular cartilage

Mark R. Buckley[a],*, Jason P. Gleghorn[b,c], Lawrence J. Bonassar[b,c], Itai Cohen[a]

[a]*Department of Physics, Cornell University, Clark Hall C7, Ithaca, NY 14853, USA*
[b]*Department of Biomedical Engineering, Cornell University, Ithaca, NY, USA*
[c]*Sibley School of Mechanical and Aerospace Engineering, Cornell University, Ithaca, NY, USA*

## Abstract

Determining the depth dependence of the shear properties of articular cartilage is essential for understanding the structure–function relation in this tissue. Here, we measured spatial variations in the shear modulus $G$ of bovine articular cartilage using a novel technique that combines shear testing, confocal imaging and force measurement. We found that $G$ varied by up to two orders of magnitude across a single sample, exhibited a global minimum 50–250 μm below the articular surface in a region just below the superficial zone and was roughly constant at depths $> 1000$ μm (the "plateau region"). For plateau strains $\gamma_{plateau} \approx 0.75\%$ and overall compressive strains $\varepsilon \approx 5\%$, $G_{min}$ and $G_{plateau}$ were $\approx 70$ and $\approx 650$ kPa, respectively. In addition, we found that the shear modulus profile depended strongly on the applied shear and axial strains. The greatest change in $G$ occurred at the global minimum where the tissue was highly nonlinear, stiffening under increased shear strain, and weakening under increased compressive strain. Our results can be explained through a simple thought model describing the observed nonlinear behavior in terms of localized buckling of collagen fibers and suggest that compression may decrease the vulnerability of articular cartilage to shear-induced damage by lowering the effective strain on individual collagen fibrils.
© 2008 Elsevier Ltd. All rights reserved.

*Keywords:* Cartilage mechanics; Shear; Depth dependence; Imaging; Collagen

## 1. Introduction

Articular cartilage is a specialized connective tissue that covers bones in diathroidal joints and transmits load across them. Its complex and inhomogeneous structure endows it with a specific mechanical response that enables it to remain effective for 6–9 decades, or most of a human lifetime. However, diseases of cartilage like osteoarthritis (OA) are common, affecting 46 million people and representing the leading cause of disability in the United States (Verbrugge, 1995). Damage to the structure of articular cartilage gives rise to disease by compromising proper functionality. Consequently, determining the complicated relationship between structure and function in this tissue is critical to understand the origin of cartilage diseases.

Articular cartilage is comprised mainly of water, type II collagen, chondrocytes and proteoglycans. These constituents are not distributed uniformly throughout the tissue. For example, collagen fibrils form a porous network with a pore density and predominant fibril orientation that vary with depth. In adult tissue, fibrils in the superficial zone tend to align parallel to the articular surface, those in the middle zone are randomly oriented and those in the deep zone are thicker and typically align perpendicular to the underlying bone (Bullough and Goodfellow, 1968). Like its structure and composition, many of the mechanical properties of articular cartilage have been shown to exhibit strong spatial variations. The depth dependence of the compressive and tensile properties of this tissue was first measured using partial thickness sectioning (Kempson et al., 1968). This technique involves cutting a full-thickness specimen of tissue into three or four pieces and testing each piece individually. It has been used, for example, to demonstrate that the strain-dependent mechanical properties of articular cartilage are manifestations of its strain- and depth-dependent properties (Chen et al., 2001).

*Corresponding author. Tel.: +1 607 255 8853; fax: +1 607 255 6428.
*E-mail addresses:* MRB45@cornell.edu (M.R. Buckley), JPG38@cornell.edu (J.P. Gleghorn), LB244@cornell.edu (L.J. Bonassar), IC64@cornell.edu (I. Cohen).

To improve spatial resolution, individual chondrocyte and local tissue deformations were measured by imaging fluorescently stained cells in cartilage samples before and after compression with a confocal microscope (Guilak et al., 1995). More recently, by using fluorescently stained chondrocyte nuclei imaged by video microscopy as markers to track tissue deformation, fine variations in the axial strain of full-thickness samples of articular cartilage were measured (Schinagl et al., 1996). In addition to adult tissue, this method was also applied to fetal and newborn bovine articular cartilage (Klein et al., 2007). These studies revealed that the compressive stiffness of articular cartilage at all stages of growth increases with depth.

On the other hand, few attempts have been made at determining spatial variations in the *shear* properties of articular cartilage. Bulk measurements of the complex shear modulus $G^*$ of articular cartilage were performed for the case of simple shear (Hayes and Bodine, 1978) and torsional shear (Zhu et al., 1993). But these studies did not determine the dependence of $G^*$ on depth $d$ from the articular surface. In another study (Eliot et al., 2002), the depth-dependent shear modulus $G(d)$ was inferred from measurements of the tensile modulus and Poisson's ratio in three 500-μm-thick partial thickness samples using the assumption of structural isotropy within each section. However, the structure of articular cartilage can vary over length scales much smaller than 500 μm. Furthermore, measurements of the physical properties of partial thickness sections of this tissue are often inconsistent with similar measurements performed on full-thickness specimens (Dumont et al., 1999). As a result, a more complete understanding of the relationship between structure and function in articular cartilage requires a more detailed measurement of the depth-dependent shear modulus.

To address this need, in this paper, we determine the dependence of the zero-frequency (i.e., equilibrium) shear modulus $G$ on depth $d$ from the articular surface with a high spatial resolution using a novel method that builds on previously demonstrated fluorescence-tracking techniques (Schinagl et al., 1996; Sveen, 2004). We then test how the shear modulus profile $G(d)$ depends on the applied axial strain and shear strain. We find that our results can be explained by a simple thought model that takes into account known variations in collagen fibril alignment within articular cartilage.

## 2. Methods

### 2.1. Sample preparation

Seven full thickness, 6 mm diameter explants were harvested sterilely from the patellofemoral groove of six 1–3-day-old calves (Gold Medal Packing, Oriskany, NY). The harvesting procedure produces cylinders with an undamaged articular surface. After dissection, samples were soaked in phosphate-buffered saline (PBS) supplemented with U/mL penicillin and 100 μ/mL streptomycin for 30 min. Each cylinder was then cut along its long axis into two hemi-cylinders, and a small section (1–3 mm) of the deep region of each hemi-cylinder was removed with a

razor blade to flatten the facet opposing the articular surface. After cutting, the average sample thickness was 3.7 mm. Stored samples were placed into Dulbecco's Modified Eagle's Medium (Invitrogen, Carlsbad, CA) supplemented with 10% fetal bovine serum (Invitrogen) at 37 °C in 5% $CO_2$ atmosphere for a maximum of 24 h. One hour before mechanical testing, explants were removed from culture and placed into a 10 μg/mL carboxyfluorescein diacetate, succinimidyl ester (Invitrogen) solution for 30 min to fluorescently stain chondrocytes within the tissue.

### 2.2. Mechanical testing

Cartilage hemi-cylinders were loaded between the two metal plates of a custom tissue deformation imaging stage (Fig. 1) that was mounted on a confocal microscope. A PBS bath ensured that the samples remained hydrated. After adhesion of the sample to the shearing plates and adjustment of the axial strain (Supplementary Section), shear deformation was induced by displacing the moveable plate in a direction parallel to the articular surface using fine-adjustment screws. Lateral shear displacements were imposed incrementally in steps of 40 μm (1–3% of the total tissue thickness), and the applied shear force was measured with a load cell (S300, Strain Measurement Devices, Meriden, CT) mounted onto the stationary plate. Samples were imaged and forces were recorded after the sample relaxed to its mechanically equilibrated state (Supplementary Section).

Imaging and tracking of fluorescently stained cells within the tissue during shear (Fig. 2, Supplementary Movie) allowed for measurement of the strain field within the tissue. Using a 10× lens with NA = 1, the field of view (636 μm × 636 μm) was always smaller than the thickness of a typical cartilage plug (≈3.7 mm). Therefore, after each increment of shear strain and subsequent force equilibration, multiple snapshots were taken throughout the sample and pieced together in order to obtain an image spanning the entire tissue.

### 2.3. Data analysis

The horizontal displacement field of cells in 317 × 40 μm² windows was calculated by performing particle image velocimetry analysis (Keane and Adrian, 1992) on confocal images before and after application of shear. The depth-dependent displacement $x(d)$ (Fig. 3A) was determined by assuming homogeneity along the direction parallel to the articular surface and averaging over all displacements in windows located at a depth $d$. The depth-dependent shear strain $\gamma(d)$ (Fig. 3B) was then extracted from $x(d)$ by computing the local slope via a five-point linear
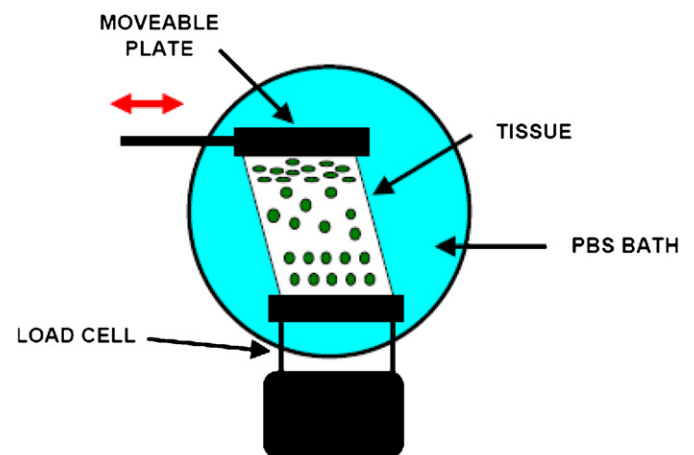


Fig. 1. Schematic representation of tissue deformation imaging stage. The device sits on the stage plate of an inverted confocal microscope, allowing the visualization of fluorescently stained cells as shear is applied.
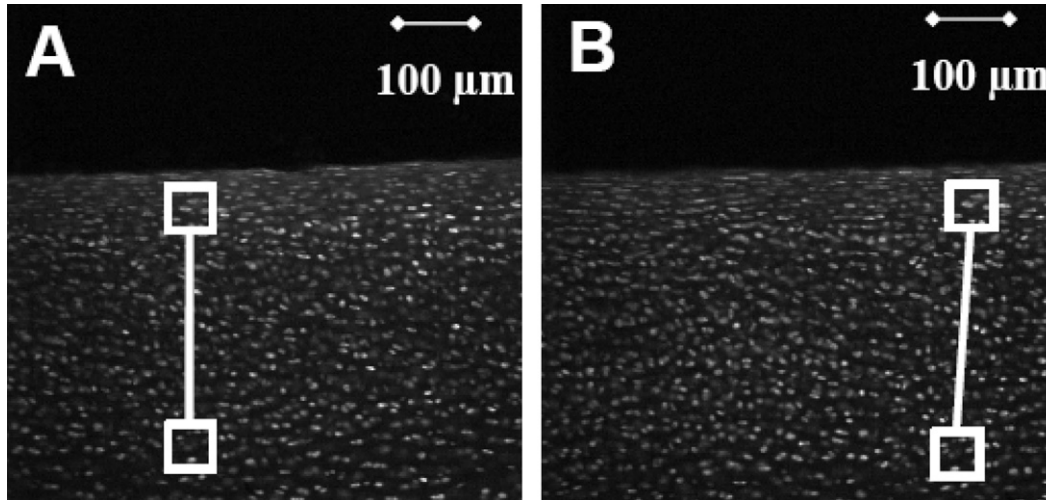
Fig. 2. Confocal micrographs taken at the surface of a sample of articular cartilage (A) before and (B) after the application of a plateau shear strain of 2.4%. Both images are 636 μm × 636 μm.

least-squares fit. Subsequently, the chord shear modulus profile (Fig. 3C) was calculated according to the equation

$$G(d) = \frac{\tau}{\gamma(d)}, \tag{1}$$

where $\tau$ is the total applied stress required to deform the tissue from zero strain to $\gamma(d)$. For each sample at a given lateral shear displacement, the parameters $\gamma_{max}$, $\gamma_{plateau}$, $G_{min}$ and $G_{plateau}$ are defined, respectively, as the maximum shear strain over the sample, the mean shear strain in the plateau region, the minimum shear modulus over the sample and the mean shear modulus in the plateau region. The "plateau region" is defined as the deep ($d > 1000$ μm) area of tissue over which the structure and mechanical properties are homogeneous. Since $\gamma(d)$ is hypothesized to be inhomogeneous and may be highly localized, $\gamma_{total}$ (i.e., the displacement of the shearing plate divided by the sample thickness) does not allow for proper comparison between samples of different thicknesses. Therefore, we report our data as a function of $\gamma_{plateau}$.

In addition to the chord shear modulus, we define the incremental (or tangential) shear modulus $G_i(d)$ to be the incremental shear stress $\Delta\tau$ divided by the incremental shear strain $\Delta\gamma(d)$ imposed on the sample so that

$$G_i(d) = \frac{\Delta\tau}{\Delta\gamma(d)}. \tag{2}$$

For a given initial and final condition, $\Delta\tau$ is measured as $\tau_{final} - \tau_{initial}$ and $\Delta\gamma(d)$ as the local *slope* of the function $\Delta x(d) = x_{final}(d) - x_{initial}(d)$. The incremental shear modulus is particularly useful for identifying stress–strain relations in nonlinear materials.

In materials with complex structures, not only is the shear strain often a nonlinear function of the shear stress, but the shear strain can also depend on the applied axial strain. In cartilage, such a dependence is logical, given that axial stress is known to modify the depth-dependent collagen architecture (Wilson et al., 2004; Quinn and Morel, 2006). In fact, previous studies have demonstrated that the torsional shear stiffness of articular cartilage is sensitive to the applied axial strain (Zhu et al., 1993). However, the connection between axial and shear strain has not been characterized. As such, we propose here an analytical scheme to describe the coupling of axial and shear strain. Based on the above discussion, it follows that the strain field, in addition to being depth dependent, will vary with $\tau$ and $\varepsilon$ such that

$$G(d) = \frac{\sigma}{\gamma(d, \tau, \varepsilon)} = \frac{\sigma}{\gamma(d, \gamma_{plateau}, \varepsilon)}, \tag{3}$$

where the second equality results from the assumption that the shear stress $\tau$ scales with the plateau shear strain $\gamma_{plateau}$. Incorporating $\gamma_{plateau}$ and $\varepsilon$

into a single parameter $\gamma_{effective}$ then gives

$$G(d) = \frac{\sigma}{\gamma(d, \gamma_{effective})}. \tag{4}$$

The simplest possible model for $\gamma_{effective}(\gamma_{plateau}, \varepsilon)$ is one with a linear dependence on $\varepsilon$, i.e.

$$\gamma_{effective} = \gamma_{plateau} + C_1\varepsilon. \tag{5}$$

In this context, $\gamma_{effective}$ can be interpreted as the shear strain in the plateau region at zero compression. The method used for determining $C_1$ is elaborated on in the results section.

### 2.4. Statistical analysis

Comparison between $G_{min}$ and $G_{plateau}$ was performed using a two-tailed paired *t*-test. $G_{min}/G_{plateau}$ for similarly tested samples was related to $\gamma_{plateau}$ and $\varepsilon$ using a repeated measures analysis of variance (ANOVA) with a Tukey test for post hoc comparison. The dependence of $G_{min}/G_{plateau}$ on $\gamma_{plateau}$ and $\gamma_{effective}$ for all tested samples was analyzed by a one-way ANOVA with a Tukey post hoc test. Differences were considered significant for $p < 0.05$.

## 3. Results

The slope of the displacement map for a typical sample of articular cartilage under a compressive strain of 2.5% and a plateau shear strain of 2.3% (Fig. 3A) was constant over a significant range of depths ($d > 500$ μm), indicative of constant shear strain. However, near the surface, the slope varied significantly. Similarly, the shear strain (Fig. 3B) and shear modulus (Fig. 3C) profiles exhibited significant spatial variations. In particular, the shear modulus exhibited a global minimum ($G_{min}$) at a depth of around 125 μm and a region of constant $G$ at $d > 500$ μm ($G_{plateau}$). We observed the same qualitative behavior as a function of depth in all studied samples. For example, the average shear modulus profile for four samples tested at $2.5\% \leqslant \gamma_{plateau} \leqslant 3.8\%$ and $3\% \leqslant \varepsilon \leqslant 5\%$ dropped to its minimum value at $d = 125$ μm and flattened out at $d > 500$ μm (Fig. 4). Similarly, four samples tested at $0.6\% \leqslant \gamma_{plateau} \leqslant 0.9\%$ and $5\% \leqslant \varepsilon \leqslant 6\%$ had distinct
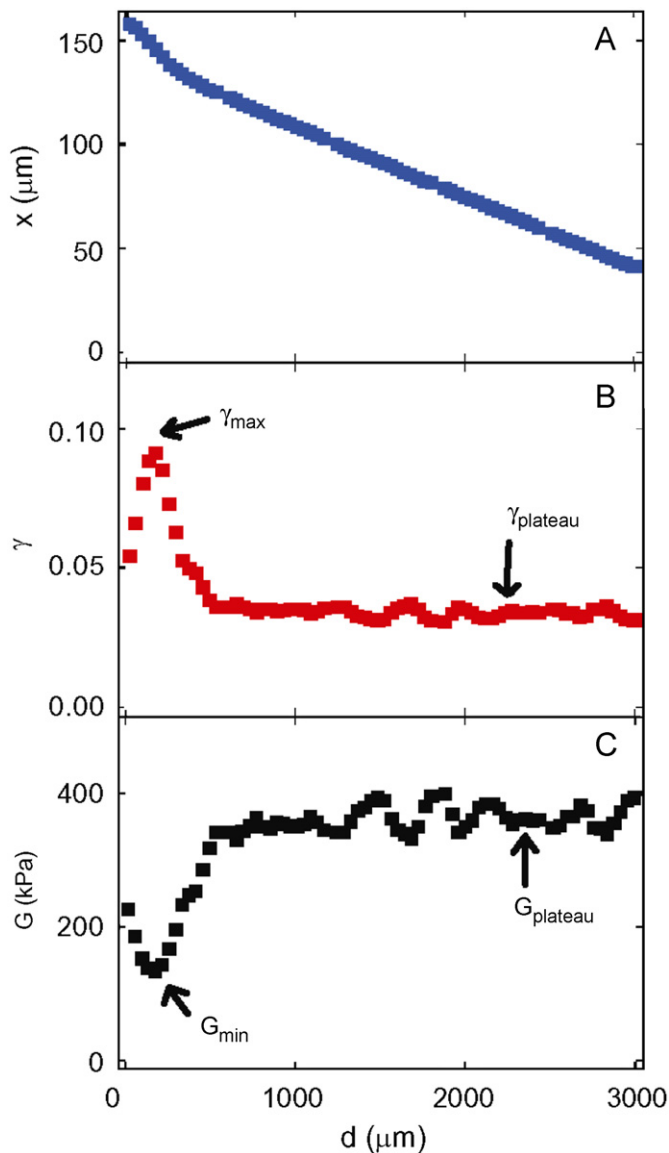
Fig. 3. Depth-dependent (A) displacement, (B) shear strain and (C) chord shear modulus for a typical sample of articular cartilage subject to a compressive strain of 2.5% and a plateau shear strain of 2.3%.



Fig. 4. Shear modulus profile for $n = 4$ samples tested at $2.5\% \leqslant \gamma_{plateau} \leqslant 3.8\%$ and $3\% \leqslant \varepsilon \leqslant 5\%$. Data are represented as mean$\pm$SD.



Fig. 5. $G_{min}$ and $G_{plateau}$ for $n = 4$ samples tested at $0.6\% \leqslant \gamma_{plateau} \leqslant 0.9\%$ and $5\% \leqslant \varepsilon \leqslant 6\%$. Data are represented as mean$\pm$SEM, $*p < 0.05$.

minima in their shear modulus profiles with $G_{min}$ roughly one-tenth of $G_{plateau}$ ($68\pm8.6$ kPa vs. $650\pm140$ kPa, $p = 0.023$) (Fig. 5).

Near the articular surface, all tested samples exhibited highly nonlinear tissue properties. In particular, in four samples of articular cartilage subject to compressive strains $5\% \leqslant \varepsilon \leqslant 6\%$, the relative stiffness of the weakest region with respect to the plateau region ($G_{min}/G_{plateau}$) increased substantially with $\gamma_{plateau}$ (Fig. 6A). Furthermore, increasing $\varepsilon$ from 2.0–2.5% to 6.0–7.5% in four samples sheared to $2.0\% \leqslant \gamma_{plateau} \leqslant 3.1\%$ decreased $G_{min}/G_{plateau}$ significantly (Fig. 6B). To further elucidate this nonlinear behavior, we have plotted shear modulus profiles for a representative sample loaded under different shear and compressive strains (Fig. 7). $G_i(d)$ in the transitional region
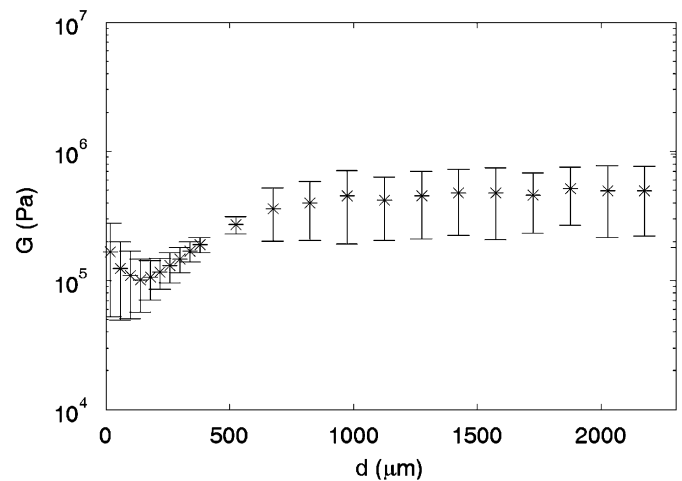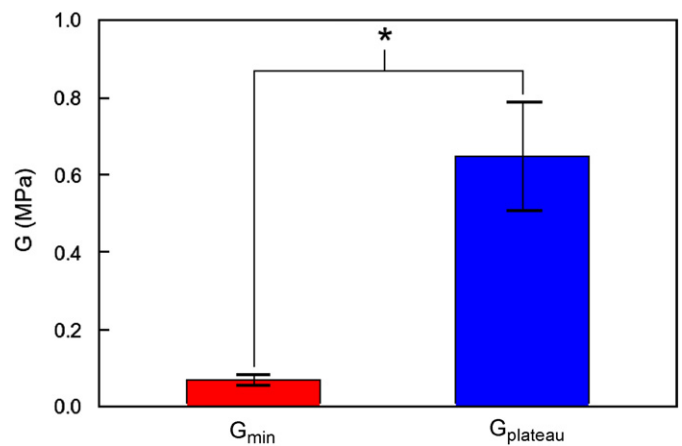
between the superficial and middle zones ($100 < d < 300 \mu m$) increased significantly with each of the three consecutive applied shear strains of $\Delta\gamma_{plateau} = 0.8\%$ (Fig. 7A). This strain stiffening was most dramatic at a depth $d = 212 \mu m$, where $G_i$ increased by about an order of magnitude, and least dramatic in the plateau region. On the other hand, increasing the axial strain from 5% to 17% decreased the incremental shear modulus near the surface of the tissue to such an extent that the minimum shear modulus (0.02 MPa) was almost two orders of magnitude smaller than the stiffest portion of the deepest region of tissue (1 MPa) under an applied strain of $\Delta\gamma_{plateau} = 0.8\%$ (Fig. 7B). This decrease was most pronounced at depths between 100 and 300 $\mu m$. Moreover, the characteristic dip in shear modulus just below the superficial zone narrowed significantly under 17% compression.

In order to account for the coupling between shear and axial strains, $G_{min}/G_{plateau}$ was compared to $\gamma_{plateau}$ for a representative sample subject to axial strains of 2.5% and 7.5% (Fig. 8A). As a result of the weakening of the
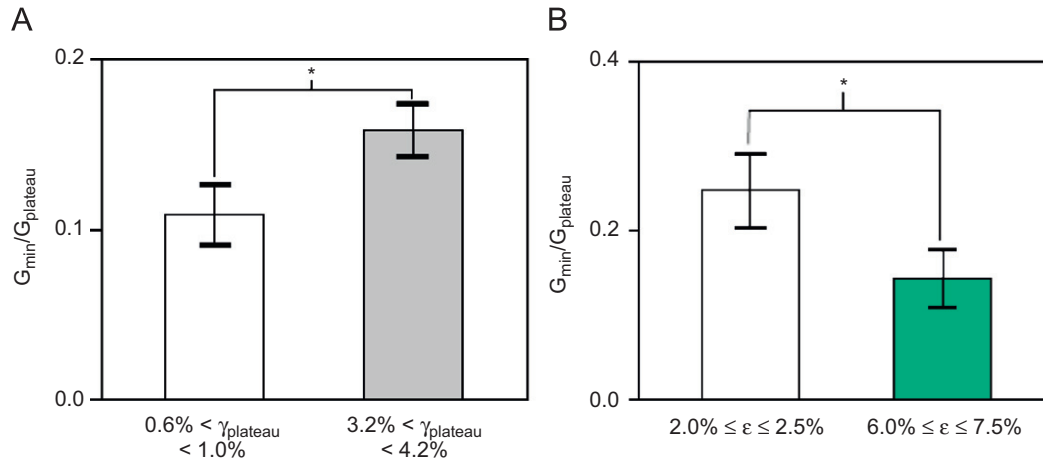
Fig. 6. (A) Ratio of minimum shear modulus to plateau shear modulus for $n = 4$ samples compressed to $5\% \leqslant \varepsilon \leqslant 6\%$ and subject to low- and high-plateau shear strains. Data are represented as mean $\pm$ SEM, $*p < 0.05$. (B) Ratio of minimum shear modulus to plateau shear modulus for $n = 4$ samples sheared to $2.0\% \leqslant \gamma_{plateau} \leqslant 3.1\%$ subject to low- and high-compressive strains $\varepsilon$. Data are represented as mean $\pm$ SEM, $*p < 0.05$.
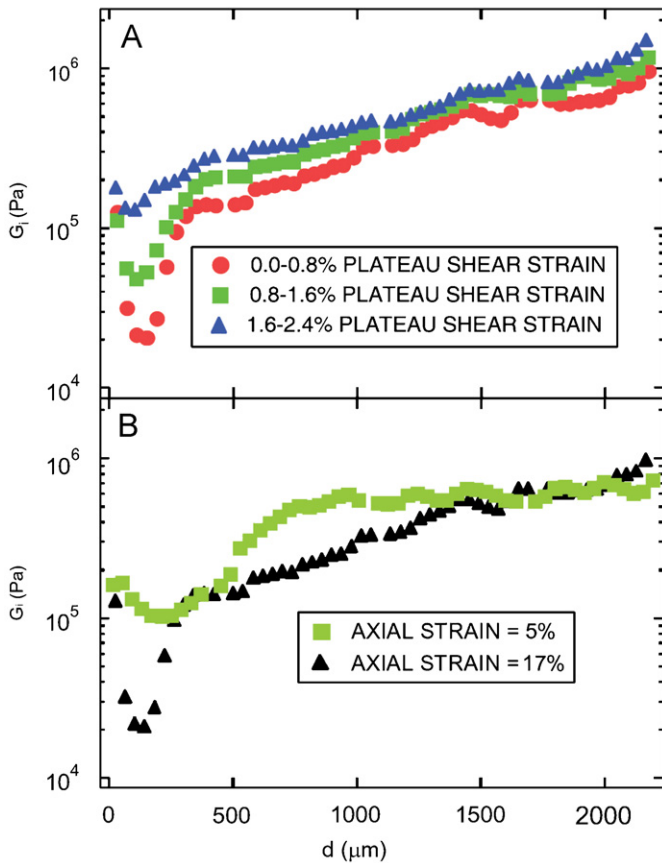


Fig. 7. (A) Incremental shear modulus vs. depth for a single representative sample of articular cartilage under an axial compression of 17% subject to three sequential applications of shear strain. (B) Incremental shear modulus vs. depth for the same sample subject to a plateau shear strain of 0.8% and compressed to axial strains of 5% and 17%.

transitional region under axial compression, $G_{min}/G_{plateau}$ was significantly lower at $\varepsilon = 2.5\%$ than at $\varepsilon = 7.5\%$. Moreover, the overlap of $G_{min}/G_{plateau}$ was most significant where the curves appear linear. Therefore, $C_1$ was

calculated by maximizing the $r^2$ value of a linear fit through $G_{min}/G_{plateau}$ vs. $\gamma_{effective}$ (Eq. (5)). Plotting $G_{min}/G_{plateau}$ against $\gamma_{effective}$ instead of $\gamma_{plateau}$ (Fig. 8B) collapsed the data onto a single curve, revealing a plateau at small values of $\gamma_{effective}$, a stiffening region at intermediate values of $\gamma_{effective}$ and a leveling off at large values of $\gamma_{effective}$. Note that this plot was shifted along the $x$-direction to ensure that the minimum value of $\gamma_{effective}$ was zero in order to compensate for the possibility of a prestrain induced in the sample while loading it into the device. The collapsed data are well characterized by a sigmoidal curve ($r^2 = 0.995$). Similarly, while the mean value of $G_{min}/G_{plateau}$ for seven tested samples did not depend significantly on $\gamma_{plateau}$ ($p = 0.088$) (Fig. 8C), the mean value of $G_{min}/G_{plateau}$ was less scattered (Fig. 8D) and increased with $\gamma_{effective}$ ($p < 10^{-7}$), where $C_1$ for each sample was calculated as described above. This result demonstrates the utility of using $\gamma_{effective}$ as a parameter allowing for comparison of samples compressed to different axial strains. Moreover, our finding that $G_{min}/G_{plateau}$ increased with $\gamma_{effective}$, while $C_1$ was negative with an average value $-0.85 \pm 0.71$ verifies that the most compliant region of tissue was stiffened by shear strain and weakened by axial strain.

## 4. Discussion

The results in this study establish that articular cartilage exhibits complex and highly inhomogeneous shear properties. $G$ exhibited a global minimum at the deep edge of the superficial zone that was significantly smaller than the shear modulus in the plateau region. In addition, the data presented above demonstrate that the shear modulus profile of articular cartilage was highly sensitive to the applied axial strain and the plateau shear strain. In particular, the region of tissue between the superficial and middle zones became stiffer under increased shear strain, and weaker under increased axial strain.
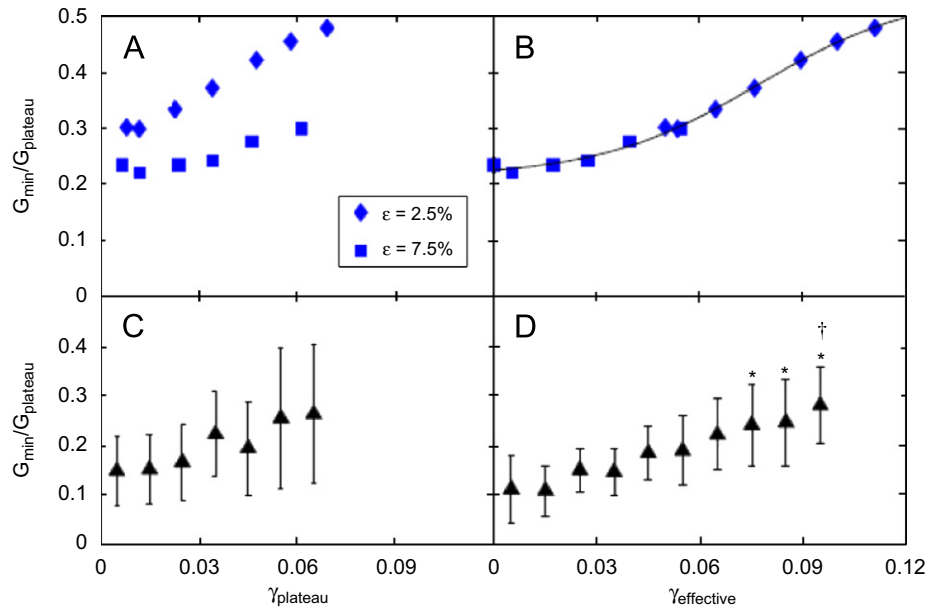
Fig. 8. Ratio of minimum shear modulus to plateau shear modulus vs. (A) plateau shear strain and (B) effective shear strain for a single representative sample. The data in (B) are well represented by a sigmoidal curve ($r^2 = 0.995$). (C) $G_{min}/G_{plateau}$ vs. plateau shear strain and (D) $G_{min}/G_{plateau}$ vs. effective shear strain. Data in (C) and (D) are represented as mean $\pm$ SD with $n = 7$, *$p < 0.05$ compared to $\gamma_{effective} = 0.005$ and 0.015, †$p < 0.05$ compared to $\gamma_{effective} = 0.025$ and 0.035.

The technique described in this study, which combines confocal imaging with controlled shear testing and force measurement, revealed variations in the functional properties of articular cartilage on the scale of 30–50 μm, most of which are concentrated within the first 500 μm of the surface. Furthermore, the value for $G_{plateau}$ ($650 \pm 140$ kPa) in samples tested at $0.6\% \leqslant \gamma_{plateau} \leqslant 0.9\%$ and $5\% \leqslant \varepsilon \leqslant 6\%$ is consistent with the value of roughly 550 kPa from previous measurements of $G$ for 1–2-week-old calf explants sheared at a low frequency (0.01 Hz) (Wilson et al., 2007).

The trends and phenomena described herein were verified in seven samples taken from six different joints. However, quantitative variations in the shear modulus profile between samples were significant (Fig. 8C and D). We surmise that these differences are due to animal–animal variation. In addition, while we did not measure split line directions in our experiments, it is possible that $G_{min}/G_{plateau}$ may be sensitive to the angle between the split line direction and the direction of shear.

According to *in situ* static loading experiments on intact human patellofemoral joints, *in vivo* strains may reach values as large as 44% (Herberhold et al., 1999). Thus, the compressive strains studied in these experiments (2–19%) were physiologically relevant. On the other hand, the current literature is unclear as to how large *in vivo* shear strains are. Nevertheless, the data presented herein indicate that even seemingly small physiological shear strains may involve much larger local shear strains in the region below the superficial zone, and axial strain exacerbates these differences. Moreover, the zero-frequency shear modulus measured in this work isolates the static aspect of the shear

response and is, therefore, a useful metric of the tissue stiffness.

In previous studies of the shear properties of articular cartilage, the first 300 μm of tissue was typically discarded in order to obtain flat samples that fit easily into standard shearing devices (Hayes and Bodine, 1978; Zhu et al., 1993). However, the current study suggests that the surface may be critical in determining the global shear properties of this tissue. Furthermore, while partial thickness sectioning studies involving the analysis of 500 μm fragments revealed the first hint of heterogeneity in the shear properties of articular cartilage (Eliot et al., 2002), the present results reveal that the length scale of this heterogeneity is in fact much smaller.

While a detailed quantitative model elucidating how the measured depth-dependent shear properties of articular cartilage arise from its inhomogeneous structure and composition remains a task for the future, we have developed a thought model that may help explain our results. In healthy articular cartilage, there is a structural transition between the aligned and densely packed collagen fibrils of the superficial zone and the randomly oriented, sparse collagen fibrils of the middle zone. Moreover, differential contrast microscopy (DIC) studies demonstrated that collagen fibers buckle most significantly in this transitional region, as evidenced by the appearance of "chevron" discontinuities just below the superficial zone in indented samples of articular cartilage (Thambyah and Broom, 2006). While these experiments were performed on adult tissue, and articular cartilage collagen architecture is known to change appreciably during development, the existence of a region with randomly oriented collagen
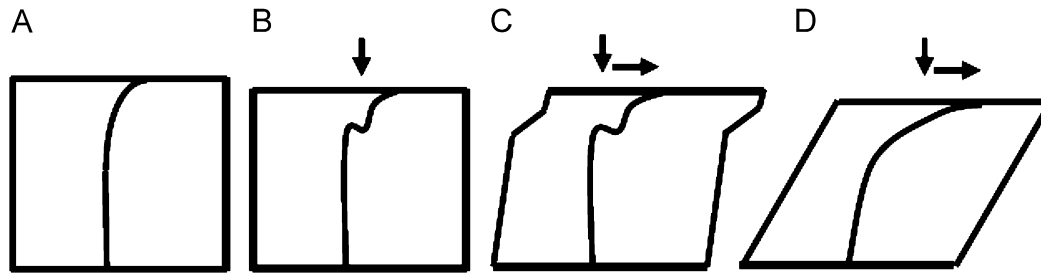
Fig. 9. Schematic representation of collagen fibrils (solid black lines) under (A) no load, (B) compression, (C) compression and early-stage shear and (D) compression and late-stage shear.

fibrils just below a superficial zone with tangentially oriented collagen fibrils has also been observed in neonatal rabbit articular cartilage specimens (Clark et al., 1997). We therefore hypothesize that the effect of small shear strains is to bend buckled collagen fibrils in the transitional region into alignment. Since collagen is much easier to bend than to stretch, this region is initially the weakest area of tissue under shear. However, once the collagen fibrils in the transitional region become aligned and taught, this region stiffens (Fig. 9). This model explains the local strain stiffening observed at depths of around 150 μm. It is also consistent with localized linear stiffening in $G_{min}/G_{plateau}$ at indermediate values of $\gamma_{plateau}$ (Fig. 8B and D). We propose that the second plateau corresponds to a regime in which all collagen fibers are fully stretched. Furthermore, additional compression should enhance the buckling of collagen fibrils, resulting in the observed decrease in shear modulus with increased axial strain and making plausible the coupling between shear and axial strain described in Eq. (5). This idea is consistent with recent theoretical investigations demonstrating that indentation or compression can alter the depth-dependent structure of the collagen network in articular cartilage and significantly reduce the strain in individual collagen fibrils oriented perpendicular to the loading direction (Wilson et al., 2004; Quinn and Morel, 2006).

The detailed, depth-dependent shear modulus profile of healthy articular cartilage suggests certain potential functional benefits. For example, the compliant region just below the superficial zone may act as an internal slip or energy dissipation mechanism, helping to maintain cartilage integrity over years of wear. Furthermore, by allowing tilt between opposing cartilage layers, this region may enhance the ability of the tissue to generate conformal joint surfaces and thereby, enhance lubrication. If, as these theories suggest, the compliance of the transitional region is associated with the durability of articular cartilage, our finding that compressive strain decreases $G$ just below the superficial zone implies that axial compression should improve resistance to wear. This conclusion is supported by previous work demonstrating that compressive strain decreases the susceptibility of articular cartilage to crack formation in the articular surface (Morel et al., 2005). However, it is also possible that the compliant region may

simply arise from a morphological or mechanical constraint during development. Future studies aimed at explaining differences in performance and durability between cartilage from different joints (e.g., the ankle and patellofemoral groove) by comparing their depth-dependent shear moduli may help to determine if there is a functional advantage of this weak region near the surface.

Since structural degradation and fibrillation due to osteoarthritis are known to be highly localized phenomena (Altman et al., 1984; Guilak et al., 1994; Hollander et al., 1995; Lark et al., 1997; Wu et al., 2002; Elsaid et al., 2003) and have been shown to begin in the superficial zone (Guilak et al., 1994; Hollander et al., 1995; Wu et al., 2002; Elsaid et al., 2003), our high-resolution method should also help elucidate how osteoarthritis progresses. In particular, it may be possible to track the progression of this disease by studying the shear properties of tissue in various stages of osteoarthritis and answer the fundamental question of how alterations to the structure of articular cartilage and its shear modulus profile precipitate disease. Similarly, it would be insightful to study the effects of injury on $G(d)$, as recent work has shown that mechanical failure is most likely to occur in the superficial zone (Morel and Quinn, 2005), perhaps as a result of the weakness of this region to shear demonstrate in this study. Furthermore, this technique may be used as a diagnostic tool for engineered cartilage and may even be extended to reveal interesting, unknown inhomogeneities in the shear properties of other types of tissue.

## Conflict of interest statement

There are no conflicts of interest to declare.

## Acknowledgments

## Appendix A. Supplementary Material

Supplementary data associated with this article can be found in the online version at doi:10.1016/j.jbiomech. 2008.05.021

## References

Altman, R.D., Tenenbaum, J., Latta, L., Riskin, W., Blanco, L.N., Howell, D.S., 1984. Biomechanical and biochemical properties of dog cartilage in experimentally induced osteoarthritis. Annals of the Rheumatic Diseases 43, 83–90.

Bullough, P., Goodfellow, J., 1968. The significance of the fine structure of articular cartilage. Journal of Bone and Joint Surgery 50, 852–857.

Chen, A.C., Bae, W.C., Schinagl, R.M., Sah, R.L., 2001. Depth- and strain-dependent mechanical and electromechanical properties of full-thickness bovine articular cartilage in confined compression. Journal of Biomechanics 34, 1–12.

Clark, J.M., Norman, A., Notzli, H., 1997. Postnatal development of the collagen matrix in rabbit tibial plateau articular cartilage. Journal of Anatomy 191, 215–227.

Dumont, J., Ionescu, M., Reiner, A., Poole, A.R., Tran-Khanh, N., Hoemann, C.D., McKee, M.D., Buschmann, M.D., 1999. Mature full-thickness articular cartilage explants attached to bone are physiologically stable over long-term culture in serum-free media. Connective Tissue Research 40, 259–272.

Eliot, D.M., Narmoneva, D.A., Setton, L.A., 2002. Direct measurement of the Poisson's ratio of human patella cartilage in tension. Journal of Biomechanical Engineering 124, 223–228.

Elsaid, K.A., Jay, G.D., Chichester, C.O., 2003. Detection of collagen type II and proteoglycans in the synovial fluids of patients diagnosed with non-infectious knee joint synovitis indicates early damage to the articular cartilage matrix. Osteoarthritis Cartilage 11, 673–680.

Guilak, F., Ratcliffe, A., Lane, N., Rosenwasser, M.P., Mow, V.C., 1994. Mechanical and biochemical changes in the superficial zone of articular cartilage in canine experimental osteoarthritis. Journal of Orthopaedic Research 12, 474–484.

Guilak, F., Ratcliffe, A., Mow, V.C., 1995. Chondrocyte deformation and local tissue strain in articular cartilage: a confocal microscope study. Journal of Orthopaedic Research 13, 410–421.

Hayes, W.C., Bodine, A.J., 1978. Flow-independent viscoelastic properties of articular cartilage matrix. Journal of Biomechanics 11, 407–419.

Herberhold, C., Faber, S., Strammberger, T., et al., 1999. *In situ* measurement of articular cartilage deformation in intact femoropatellar joints under static loading. Journal of Biomechanics 32, 1287–1295.

Hollander, A.P., Pidoux, I., Reiner, A., Rorabeck, C., Bourne, R., Poole, A.R., 1995. Damage to type II collagen in aging and osteoarthritis starts at the articular surface, originates around chondrocytes, and extends into the cartilage with progressive degeneration. Journal of Clinical Investigation 96, 2859–2869.

Keane, R.D., Adrian, R.J., 1992. Theory of cross correlation analysis of PIV images. Applied Scientific Research 49, 191–215.

Kempson, G.E., Freeman, M.A.R., Swanson, S.A.V., 1968. Tensile properties of articular cartilage. Nature 20, 1127–1128.

Klein, T.J., Chaudhry, M., Bae, W.C., Sah, R.L., 2007. Depth-dependent biomechanical and biochemical properties of fetal, newborn, and tissue-engineered articular cartilage. Journal of Biomechanics 40, 182–190.

Lark, M.W., Bayne, E.K., Flanagan, J., Harper, C.F., Hoerrner, L.A., Hutchinson, N.I., Singer, I.I., Donatelli, S.A., Weidner, J.R., Williams, H.R., Mumford, R.A., Lohmander, L.S., 1997. Aggrecan degradation in human cartilage. Journal of Clinical Investigation 100, 93–106.

Morel, V., Quinn, T.M., 2005. Short-term changes in cell and matrix damage following mechanical injury of articular cartilage explants and modeling of microphysical mediators. Biorheology 41, 509–519.

Morel, V., Mercay, M.Sc., Quinn, T.M., 2005. Prestrain decreases cartilage susceptibility to injury by ramp compression *in vitro*. Osteoarthritis and Cartilage 13, 964–970.

Quinn, T.M., Morel, V., 2006. Microstructural modeling of collagen network mechanics and interactions with the proteoglycan gel in articular cartilage. Biomechanics and Modeling in Mechanibiology 6, 73–82.

Schinagl, R.M., Ting, M.K., Price, J.H., Sah, R.L.-Y., 1996. Video microscopy to quantitate the inhomogeneous equilibrium strain within articular cartilage during confined compression. Annals of Biomedical Engineering 24, 500–512.

Sveen, J.K., 2004. An introduction to MatPIV v. 1.61. In: Mechanics and Applied Mathematics, Department of Mathematics, University of Oslo, (e-print series), No. 2 ISSN 0809-4403.

Thambyah, A., Broom, N., 2006. Micro-anatomical response of cartilage-on-bone to compression: mechanisms of deformation within and beyond the directly loaded matrix. Journal of Anatomy 209, 611–622.

Verbrugge, L.M., 1995. Women, men and osteoarthritis. Arthritis Care and Research 8, 212–220.

Wilson, W., van Donkelaar, C.C., van Rietbergen, B., Ito, K., Huiskes, R., 2004. Stresses in the local collagen network of articular cartilage: a poroviscoelastic fibril-reinforced finite element study. Journal of Biomechanics 37, 357–366.

Wilson, C.G., Palmer, A.W., Zuo, F., Eugui, E., Wilson, S., Mackenzie, R., Sandy, J.D., Levenston, M.E., 2007. Selective and non-selective metalloproteinase inhibitors reduce Il-1-induced cartilage degradation and loss of mechanical properties. Matrix Biology 26, 259–268.

Wu, W., Billinghurst, R.C., Pidoux, I., Antoniou, J., Zukor, D., Tanzer, M., Poole, A.R., 2002. Sites of collagenase cleavage and denaturation of type II collagen in aging and osteoarthritic articular cartilage and their relationship to the distribution of matrix metalloproteinase 1 and matrix metalloproteinase 13. Arthritis and Rheumatism 46, 2087–2094.

Zhu, W., Mow, V.C., Koob, T.J., Eyre, D.R., 1993. Viscoelastic shear properties of articular cartilage and the effects of glycosidase treatments. Journal of Orthopaedic Research 11, 771–781.